Collision Avoidance for Underactuated Marine Vehicles Using the Constant Avoidance Angle Algorithm

Martin S. Wiig, *Member, IEEE,* Kristin Y. Pettersen, *Fellow, IEEE,* and Thomas R. Krogstad, *Member, IEEE*

***Abstract*—Avoiding collisions is a crucial ability for unmanned vehicles. In this paper, we present the constant avoidance angle algorithm, a reactive method for collision avoidance. It can be used to avoid both static and moving obstacles by making the vehicle keep an avoidance angle between itself and the obstacle edge. Unlike many other algorithms, it requires neither knowledge of the complete obstacle shape, nor that the vehicle follows a desired speed trajectory. Rather, safe vehicle headings are provided at the current vehicle speed. Thus, the speed can be used as an input to the algorithm, which provides flexibility and makes the approach suitable for a wide range of vehicles, including vehicles with a limited speed envelope or high acceleration cost. We demonstrate this by applying the algorithm to a marine vehicle described by a full kinematic and dynamic model in three degrees of freedom. We specifically consider vehicles with underactuated sway dynamics, where the vehicle velocity contains a component which cannot be directly controlled. Such dynamics can be highly detrimental to the performance of collision avoidance algorithms, and need to be included in the design and analysis of control systems for such vehicles. In this paper, we compensate for the underactuation by including these dynamics in the underlying analysis and control design. We provide a mathematical analysis of sparse obstacle scenarios, where we derive conditions under which safe avoidance is guaranteed, even for underactuated vehicles. We furthermore show how the modular nature of the algorithm enables it to be combined both with a target reaching and a path following guidance law. Finally, we validate the results both through numerical simulations, and through full-scale experiments aboard the R/V Gunnerus.**

***Index Terms*—Collision avoidance, marine vehicles, nonlinear dynamical systems, underactuated systems**

I. Introduction

Unmanned marine vehicles are increasingly employed in tasks like transportation, seafloor mapping, oceanographic surveying or ocean surveillance [1], [2]. Such systems encounter challenges like limited maneuverability, reduced or delayed communications and resulting lack of real-time operator control. Thus, safety critical functions such as collision avoidance are crucial for operational success.

We will in this paper consider a class of *underactuated* marine vehicles, specifically vehicles with control actuation in the forward direction and in the vehicle heading, but not in the sideways direction. This class of vehicles includes a wide range of displacement vessels operating at maneuvering speed [3]. While the sideways (sway) movement cannot be directly controlled for such vehicles, it is induced during turning. It thus becomes an important factor to consider in the design and analysis of collision avoidance algorithms for such vehicles.

Surveys of recent progress within collision avoidance algorithms can be found in [4]–[6]. In general, the different algorithms can be divided into two families; motion planning algorithms like model predictive control [7]–[9] or the faster dynamic window algorithm [10]–[12], and reactive algorithms.

Motion planning algorithms create optimal and safe paths using a vehicle model and an environment model. However, the general motion planning problem has been shown to be NP-hard [13]. Thus, even if the computational cost can be reduced by limiting the control inputs to a small set of discrete values [7], [8], the approach can still be intractable for vehicles with limited processing. Furthermore, even systems capable of running a motion planning algorithm will benefit from having another, computationally fast, algorithm as a backup for redundancy. Hence, there is a need for reactive algorithms.

The artificial potential field (APF) method [14], which guides the vehicle using repulsive and attractive fields, is intuitive and straightforward to implement even for complex environments. Furthermore, different fields can be combined in order to achieve simultaneous goals like formation control and obstacle avoidance [15]. Stability issues has been identified with the algorithm [16], which can be countered by extending the algorithm to the polar domain as in the vector field histogram [17]. These methods only consider static obstacles, though, and there are no safety guarantees.

Representing the obstacle in the velocity space is the main idea behind the velocity obstacle (VO) approach [18]. By choosing a vehicle velocity outside of the set of velocity obstacles, algorithms implementing velocity obstacles inherently include moving obstacles. The approach can be extended to include traffic rules such as the International regulations for preventing collisions at sea (COLREGS) [19].

While the original formulation of the VO algorithm assumes that the vehicle is fully actuated, and does not include vehicle dynamics, the acceleration VO [20] also includes acceleration constraints. The approach can be further extended to include unicycle-type nonholonomic constraints, but becomes restrictive if the forward acceleration or turning rate the vehicle is limited. The complete vehicle dynamics are included in the

This work was partly supported by the Research Council of Norway through the Centres of Excellence funding scheme, project no. 223254 - NTNU AMOS

M. S. Wiig and K. Y. Pettersen are with the Centre for Autonomous Marine Operations and Systems (NTNU AMOS), Department of Engineering Cybernetics, Norwegian University of Science and Technology, Trondheim, Norway, {Martin.Wiig,Kristin.Y.Pettersen}@ntnu.no

M. S. Wiig, K. Y. Pettersen and T. R. Krogstad are with the Norwegian Defence Research Establishment, Kjeller, Norway, Thomas-Robekk.Krogstad@ffi.no

generalized VO [21], which represents the obstacles in the control input space. However, the calculation of this space is not trivial, and can be computationally expensive.

In [22] the collision cone concept [23] is employed in a distributed reactive algorithm for multiple vehicles. The algorithm provably makes a set of cooperating vehicles remain collision free if they start in a conflict free state, and a deconfliction algorithm for reaching such a state is given. The algorithm incorporates actuator constraints, and is suitable also for vehicles with a limited speed envelope. However, while the results are strong, the dynamics of the vehicles are not included, and the conditions for safe deconfliction can become overly conservative in the case of passive obstacles.

The algorithm proposed by [24] uses circular path following to avoid moving obstacles, and the paper gives sufficient conditions for successful avoidance. By using set-based theory to switch between path following mode and collision avoidance mode, the algorithm is combined with the popular line-of-sight guidance law [25] for following of straight line path segments. This path following algorithm is used as an example also in our paper, and is described in Section V-B. It is not, however, clear how to extend the algorithm of [24] to noncircular obstacles, nor is a minimum distance for when the vehicle should start the collision avoidance maneuver provided.

The constant avoidance angle (CAA) algorithm was first proposed in [26]. The algorithm provably avoids a moving obstacle by steering the vehicle a constant avoidance angle to the side of it. There is, however, no consideration of any underlying vehicle dynamics in the analysis of the algorithm. Furthermore, the vehicle is subject to considerable forward acceleration during the collision avoidance maneuver, and can be brought to a complete stop. The algorithm can thus become unsuitable for vehicles with forward acceleration constraints or a limited speed envelope.

In this paper, the CAA algorithm is modified to accommodate such vehicles by setting the forward speed as an input rather than an output of the algorithm, thus making it possible to steer the forward speed independently. As an example, we will allow the vehicle to keep a constant forward speed during the maneuver. The vehicle thus both adheres to the heavy forward acceleration cost of many marine vehicles, and becomes more predictable for an external observer. Preliminary results were presented in [27], which only considered vehicle kinematics, and in [28], where the CAA algorithm was further extended to include the underactuated dynamics of the vehicle sway motion.

In this paper, the results are extended to a vehicle modeled using a complete maneuvering model [3]. This includes both the underactuated sway dynamics and the directly actuated yaw and surge dynamics. The underactuated sway dynamics will be accounted for by making the algorithm steer the vehicle course rather than the vehicle heading. As the vehicle turns, the induced sway motion will add a sideways component to the vehicle's velocity, and the magnitude of the total speed varies during the maneuver. However, since the vehicle speed is now used as an input to the algorithm, the adjusted course will be adjusted accordingly in order to remain provably safe. Moreover, we will show that the resulting course reference is well defined by proving that the sway motion remains bounded. Finally, we will show how smoothing of the desired yaw rate using a simple, linear bump function can be used to extend the algorithm to be applicable on a vehicle model including forces and moments in all three degrees of freedom. Thus, we demonstrate in this paper that the CAA algorithm is applicable to an underactuated marine vehicle modeled with forces and moments in all three degrees of freedom.

We will demonstrate the modular nature of the proposed collision avoidance law by giving conditions for safe navigation when coupled with both a pure pursuit target reaching guidance law [29], [30], as well as with the popular line of sight path following guidance law [25], [31]. Target reaching and path following can be used to achieve a wide array of high level goals, such as transit, pipeline inspection, sea floor mapping or monitoring of autonomous underwater vehicles. Hence, by showing that the proposed algorithm can be combined with these guidance laws, we show that it can increase vehicle safety in many different operational scenarios. The results are validated through both numerical simulations and through full-scale experiments on the R/V Gunnerus.

The analysis of the algorithm considers a single moving obstacle of circular shape. However, the algorithm can be used to avoid an obstacle of any shape without any modification, which we demonstrate in the simulation section. Furthermore, while the analysis of dense multi-obstacle scenarios is beyond the scope of this paper, we will provide a method for extending the algorithm to such scenarios. This is demonstrated in the experimental section, where we validate the results through the experiments on R/V Gunnerus.

The remainder of this paper is organized as follows: The vehicle model is given in Section II, while the obstacle is described in Section III. The CAA collision avoidance algorithm is presented in Section IV, and the target reaching and path following guidance laws are given in Section V. The controller used to follow the course references from these algorithms is presented in Section VI, which includes the smoothing function ensuring that the resulting yaw rate reference trajectory is feasible. The surge and yaw rate controllers are presented in Section VII. A mathematical analysis of the system is provided in Section VIII, which gives conditions of provable safe maneuvering. The results are validated through simulations in Section IX and experiments in Section X, before some concluding remarks are given in Section XI.

II. Vehicle model

We model the vehicle in 3 degrees of freedom (DOF), with the position and orientation of the vehicle's body frame b in the inertial NED frame n denoted $\boldsymbol{p}_b^n \triangleq [x_b^n, y_b^n]$ and ψ_b^n, respectively. The linear and angular velocity of b with respect to n is denoted $\boldsymbol{\nu}_{b/n}^b \triangleq [u_b, v_b, r_b]^T$, where u_b is the forward (surge) speed, v_b is the sideways (sway) speed and r_b is the angular velocity of the vehicle (the yaw rate). The kinematics of the vehicle can then be written as

$$\dot{\boldsymbol{\eta}}_b = \boldsymbol{J}_b^n(\psi_b^n)\boldsymbol{\nu}_{b/n}^b, \tag{1}$$

where $\boldsymbol{\eta}_b \triangleq [x_b^n, y_b^n, \psi_b^n]^T$ and the transformation matrix $\boldsymbol{J}_b^n$ is

$$\boldsymbol{J}_b^n(\psi_b^n) \triangleq \begin{bmatrix} \boldsymbol{R}_b^n(\psi_b^n) & 0 \\ 0 & 1 \end{bmatrix}.$$

The dynamics of the vehicle are modeled using the maneuvering model of [3]:

$$\boldsymbol{M}\dot{\boldsymbol{\nu}}_{b/n}^b + \boldsymbol{C}(\boldsymbol{\nu}_{b/n}^b)\boldsymbol{\nu}_{b/n}^b + \boldsymbol{D}\boldsymbol{\nu}_{b/n}^b = \boldsymbol{B}\boldsymbol{f}. \tag{2}$$

The symmetric mass matrix $\boldsymbol{M} > 0$ contains the mass, inertia and hydrodynamic added mass of the vehicle. Coriolis and centripetal terms are contained in $\boldsymbol{C}$, while the $\boldsymbol{D}$ is the linear hydrodynamic damping matrix. The vector $\boldsymbol{f} \triangleq [T_u, T_r]^T$ contains the surge thrust T_u and rudder angle T_r, which actuates the system through the configuration matrix $\boldsymbol{B} \in \mathbb{R}^{3\times 2}$.

The system matrices have the following structure [3]:

$$\boldsymbol{M} \triangleq \begin{bmatrix} m_{11} & 0 & 0 \\ 0 & m_{22} & m_{23} \\ 0 & m_{23} & m_{33} \end{bmatrix}, \tag{3}$$

$$\boldsymbol{C} \triangleq \begin{bmatrix} 0 & 0 & -m_{22}v_b - m_{23}r_b \\ 0 & 0 & m_{11}u_b \\ m_{22}v_b + m_{23}r_b & -m_{11}u_b & 0 \end{bmatrix}, \tag{4}$$

$$\boldsymbol{D} \triangleq \begin{bmatrix} d_{11} & 0 & 0 \\ 0 & d_{22} & d_{23} \\ 0 & d_{32} & d_{33} \end{bmatrix}, \quad \boldsymbol{B} \triangleq \begin{bmatrix} b_{11} & 0 \\ 0 & b_{22} \\ 0 & b_{33} \end{bmatrix}. \tag{5}$$

This structure is obtained by using the following assumption, which holds for most marine vehicles:

Assumption 1. *The vehicle is port-starboard symmetric.*

Since the vehicle dynamics (2) are described using a maneuvering model, we assume that the vehicle operates at maneuvering speed:

Assumption 2. *The vehicle surge speed u_b lies in the interval $u_b \in [u_{b,\min}, u_{b,\max}]$, where $u_{b,\min} > 0$ and $u_{b,\max} \geq u_{b,\min}$ are constant parameters.*

In the model (2), the yaw control T_r affects not only the yaw dynamics but also the underactuated sway dynamics, complicating the controller design. To make the control problem more feasible, we remove the control input T_r from the sway dynamics. This is done through the following assumption:

Assumption 3. *The origin of b is located in a point $[x_{bg}, 0]^T$ along the centerline of the vessel, and this point is the pivot point of the ship.*

Assumption II makes $\boldsymbol{M}^{-1}\boldsymbol{B}\boldsymbol{f} = [\tau_u, 0, \tau_r]^T$, where τ_u is the control force in surge and τ_r is the control moment in yaw. As described in [3], it is always possible to use a coordinate transformation on b in order to translate the origin to the pivot point, should it not be located there originally.

A. Expanded kinematics and dynamics

For clarity, we expand the vehicle kinematics (1) and dynamics (2) into their separate components:

$$\dot{x}_b^n = u_b\cos(\psi_b^n) - v_b\sin(\psi_b^n), \tag{6a}$$
$$\dot{y}_b^n = u_b\sin(\psi_b^n) + v_b\cos(\psi_b^n), \tag{6b}$$
$$\dot{\psi}_b^n = r_b, \tag{6c}$$
$$\dot{u}_b = F_{u_b}(u_b, v_b, r_b) + \tau_u, \tag{6d}$$
$$\dot{v}_b = X(u_b)r_b + Y(u_b)v_b, \tag{6e}$$
$$\dot{r}_b = F_{r_b}(u_b, v_b, r_b) + \tau_r. \tag{6f}$$

The functions $F_u(v_b, r_b)$, $X(u_b)$, $Y(u_b)$ and $F_r(u_b, v_b, r_b)$ contain mass and damping parameters, and are defined in Appendix A. To ensure that the vehicle is nominally stable in sway (6e), we make the following assumption on $Y(u_b)$:

Assumption 4. *The function $Y(u_b)$ satisfies*

$$Y(u_b) < 0. \tag{7}$$

If Assumption 4 does not hold, then a small disturbance in sway would lead to a steadily increasing sway motion, which is not the case for commercial vessels by design.

B. The flow frame

The linear vehicle velocity, $\boldsymbol{v}_{b/n}^b \triangleq [u_b, v_b]^T$, contains a forward and sideways velocity component. However, for collision avoidance purposes, we are interested in the magnitude and direction of $\boldsymbol{v}_{b/n}^b$. This can be expressed through the flow frame f, which is a body-fixed frame rotated so that its x-axis is aligned with the flow of water around the vehicle [3]. The rotation from body to flow is given by $\boldsymbol{R}_f^b(\beta)$, where the sideslip angle β is defined as $\beta \triangleq \tan^{-1}(v_b/u_b)$. Hence, the vehicle kinematics can be expressed as

$$\dot{\boldsymbol{p}}_{b/n}^n = \boldsymbol{R}_b^n(\psi_b^n)\boldsymbol{R}_f^b(\beta)\boldsymbol{v}_{b/n}^f = \boldsymbol{R}_f^n(\psi_f^n)\boldsymbol{v}_{b/n}^f, \tag{8}$$

where $\psi_f^n \triangleq \psi_b^n + \beta$ is termed the vehicle course, the velocity in f is $\boldsymbol{v}_{b/n}^f \triangleq [U_b, 0]^T$, and $U_b \triangleq \sqrt{u_b^2 + v_b^2}$. The course rate r_f is found by taking the time derivative of β and inserting for $\dot{v}_b$, which is given by (6e):

$$r_f \triangleq \dot{\psi}_f^n = \frac{\left(X(u_b)u_b + U_b^2\right)r_b + Y(u_b)u_b v_b - \dot{u}_b v_b}{U_b^2}. \tag{9}$$

The expression for $\dot{v}_b$ as a function of r_f is found as

$$\dot{v}_b = \frac{U_b^2\left(X(u_b)r_f + Y(u_b)v_b\right)}{X(u_b)u_b + U_b^2} + \frac{X(u_b)v_b\dot{u}_b}{X(u_b) + U_b^2}. \tag{10}$$

In order for (10) to be well defined, the following assumption needs to be met [32]:

Assumption 5. *The function $X(u_b)$ satisfies*

$$X(u_b) + u_b > 0 \quad \forall\ u_b \in [u_{b,\min}, u_{b,\max}]. \tag{11}$$

Remark 1. *This assumption ensures that a change in the vehicle heading ψ_b^n will result in a change in the vehicle course in the nominal case when $\dot{u}_b = 0$. This is the case for most marine vehicles by design.*

C. Desired surge speed

The surge speed u_b will be controlled by using the feedback linearizing controller described in Section VII to reach a desired surge speed u_{bd}. In this paper, we set the desired surge speed to a positive constant:

Assumption 6. *The desired surge speed is constant and satisfies* $u_{bd} > 0$.

For brevity, we introduce the notation $X_{\mathrm{d}} \triangleq X(u_{bd})$ and $Y_{\mathrm{d}} \triangleq Y(u_{bd})$.

III. Obstacle Model

In this section we will describe the obstacle model, as well as the obstacle measurements required to implement the collision avoidance algorithm described in Section IV.

The obstacle is modeled as a moving circular domain $\mathcal{D}_o$ with radius R_o:

$$\dot{\boldsymbol{p}}_o^n = \boldsymbol{R}_o^n(\psi_o^n)\boldsymbol{v}_{o/n}^o, \tag{12}$$

where $\boldsymbol{p}_o^n \triangleq [x_o^n, y_o^n]^T$ are the Cartesian coordinates of the obstacle, the obstacle-fixed velocity is contained in $\boldsymbol{v}_{o/n}^o \triangleq [u_o, 0]$, and the obstacle heading is denoted ψ_o^n.

Remark 2. *The proposed collision avoidance algorithm can also be applied to non-circular obstacles, which is demonstrated in a simulation in Section IX.*

To ensure that the vehicle is able to circumvent the obstacle, we need to assume that the obstacle speed is less than the desired vehicle surge speed. The obstacle speed is further restricted if a large vehicle sway speed is induced towards the obstacle when the vehicle turns away from it, i.e. if the maneuvering capabilities of the vehicle is poor. This restriction comes from the mathematical analysis in Section VIII.

Assumption 7. *The obstacle forward speed* u_o *is upper bounded by*

$$u_o < \begin{cases} 2\sqrt{-X_d^2 - X_d u_{bd}} & -u_{bd} < X_d \leq -\frac{u_{bd}}{2} \\ u_{bd} & -\frac{u_{bd}}{2} < X_d. \end{cases} \tag{13}$$

A. Required obstacle measurements

In order to decide when to start an avoidance maneuver, the vehicle must be able to sense the distance $d_{ob} \triangleq \|\boldsymbol{p}_b^n - \boldsymbol{p}_o^n\|$ to the obstacle. To obtain a safe course, the vehicle must furthermore be able to sense the vision cone $\mathcal{V}$ to the obstacle, as illustrated in Fig. 1. Specifically, the angles $\alpha^{(1)}$ and $\alpha^{(2)}$ to the edges of the $\mathcal{V}$ are required. Finally, the vehicle must know the obstacle velocity $\dot{\boldsymbol{p}}_o^n$ in order to compensate for it.

Remark 3. *The obstacle distance* d_{ob} *and the vision cone can be readily obtained from sensors such as a lidar, radar or sonar. If the sensor has Doppler capabilites, the obstacle velocity is available as well. Otherwise, the obstacle velocity can be obtained by using a tracking algorithm.*

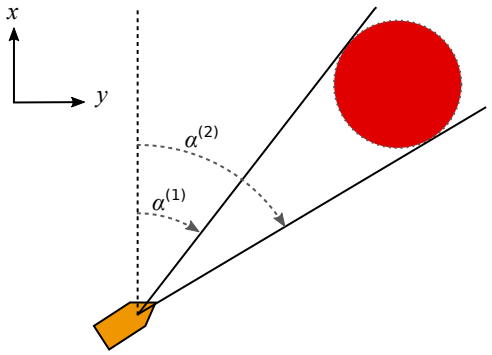

Fig. 1. The vision cone $\mathcal{V}$ from the vehicle to the obstacle.

IV. Collision avoidance algorithm

In this section we will describe the proposed constant avoidance angle (CAA) algorithm for collision avoidance. We define that the control system will be either in nominal guidance mode, where it follows a nominal guidance law like the ones we describe in Section V, or in collision avoidance mode. The control system will enter collision avoidance mode if the vehicle comes at risk of colliding with an obstacle, according to a criterion we will define in Section IV-B. The CAA algorithm will then make the vehicle circumvent the obstacle by steering the vehicle outside of the vision cone $\mathcal{V}$ defined in Section III-A. Specifically, by maintaining a constant avoidance angle α_{o} to the vision cone, it is ensured that the vehicle will not come within a specified minimum distance of the obstacle. If the obstacle is moving, a compensation term is adding to the avoidance angle.

During the collision avoidance maneuver, a sway motion will be induced as the vehicle turns. Thus, unlike for vehicles with unicycle kinematics, the vehicle heading ψ_b^n is not necessarily aligned with the vehicle course ψ_f^n. Hence we will make the CAA algorithm provide course rather than heading references. These references will be used as input to the course controller we propose in Section VI, which will then create smooth reference trajectories for the yaw rate controller described in Section VII. We are thus able to include the complete vehicle dynamics in the analysis in Section VIII.

The desired course during collision avoidance, including the compensation for the obstacle velocity, is described in detail in Section IV-A below. The rules for entering and leaving collision avoidance mode are given in Section IV-B, while finally an example rule for deciding if the vehicle should move to the port or starboard side of the obstacle is given in Section IV-C.

A. Desired vehicle course

To create course references that will safely avoid the obstacle, the CAA algorithm extends the vision cone $\mathcal{V}$ by $\pm\alpha_{\mathrm{o}}$ to either side, as shown in Fig. 2. The heading angles of the extended vision cone edges are denoted $\psi_{\alpha_{\mathrm{o}}}^{(1)}$ and $\psi_{\alpha_{\mathrm{o}}}^{(2)}$. Two velocity vectors, $\boldsymbol{v}_{\alpha_{\mathrm{o}}}^{(1)}$ and $\boldsymbol{v}_{\alpha_{\mathrm{o}}}^{(2)}$, are defined along the edges of the extended cone:

$$\boldsymbol{v}_{\alpha_{\mathrm{o}}}^{(j)} \triangleq u_{\alpha_{\mathrm{o}}} \left[\cos(\psi_{\alpha_{\mathrm{o}}}^{(j)}), \sin(\psi_{\alpha_{\mathrm{o}}}^{(j)})\right], \; j = \{1, 2\}, \tag{14}$$

Dette er en postprint-versjon/This is a postprint version. Publisert versjon/Publised version: https://doi.org/10.1109/TCST.2019.2903451

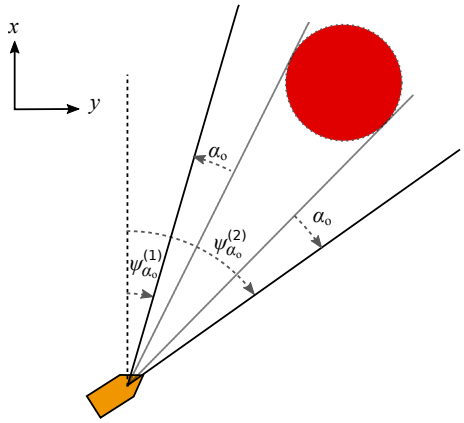

Fig. 2. The extended vision cone from the vehicle to the obstacle.

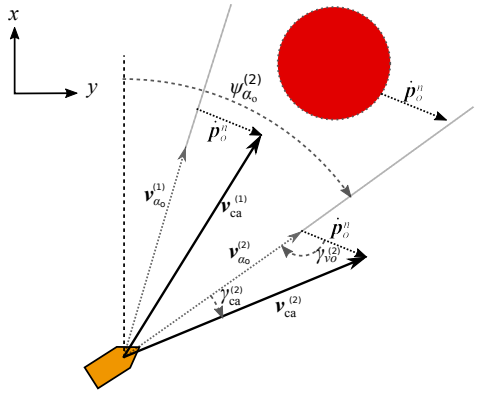

Fig. 3. The desired velocity vector candidates $\boldsymbol{v}_{\text{ca}}^{(1)}$ and $\boldsymbol{v}_{\text{ca}}^{(2)}$, which define the sides of the compensated vision cone $\mathcal{V}_{\text{c}}$.

where $u_{\alpha_o} > 0$ will be defined later.

If the obstacle is moving, each edge of the extended vision cone will be rotated around the origin of b in order to compensate for the obstacle velocity. Thus, in a reference frame aligned with n but moving with the obstacle, the course references of the CAA algorithm will follow $\boldsymbol{v}_{\alpha_o}^{(j)}$. The rotated edges define a new, compensated vision cone $\mathcal{V}_{\text{c}}$, which is illustrated in Fig. 3. Two velocity vectors are defined along the edges of $\mathcal{V}_{\text{c}}$ as

$$\boldsymbol{v}_{\text{ca}}^{(j)} \triangleq \boldsymbol{v}_{\alpha_o}^{(j)} + \dot{\boldsymbol{p}}_o^n, \quad j = \{1, 2\}. \tag{15}$$

The velocity vectors $\boldsymbol{v}_{\text{ca}}^{(j)}$ will keep the constant avoidance angle α_o to the obstacle, and will hence be used as candidates for the desired vehicle velocity in collision avoidance mode. Therefore, their lengths are set to the current vehicle speed U_b,

$$||\boldsymbol{v}_{\text{ca}}^{(j)}|| \triangleq U_b. \tag{16}$$

The compensation angle $\gamma_{\text{ca}}^{(j)}$ is found using the sine rule on the triangle defined by $\boldsymbol{v}_{\alpha_o}^{(j)}$, $\dot{\boldsymbol{p}}_o^n$ and $\boldsymbol{v}_{\text{ca}}^{(j)}$:

$$\gamma_{\text{ca}}^{(j)} = \sin^{-1}\left(\frac{\|\dot{\boldsymbol{p}}_o^n\| \sin(\gamma_{vo}^{(j)})}{U_b}\right), \; j = \{1, 2\}. \tag{17}$$

where $\|\dot{\boldsymbol{p}}_o^n\| = u_o$ as seen in (12). The angle $\gamma_{vo}^{(j)}$ is found geometrically as

$$\gamma_{vo}^{(j)} = \pi - (\psi_o^n - \psi_{\alpha_o}^{(j)}), \; j = \{1, 2\}. \tag{18}$$

The candidates for desired vehicle course in collision avoidance mode are then defined as

$$\psi_{f\text{dca}}^{n(j)} \triangleq \psi_{\alpha_o}^{(j)} + \gamma_{\text{ca}}^{(j)}, \; j = \{1, 2\}. \tag{19}$$

Section IV-C provides a rule for choosing between these two candidates.

B. Switching rule

The compensated vision cone $\mathcal{V}_{\text{c}}$ is used to define a set of unsafe vehicle course directions. Thus, we define that the control system enters collision avoidance mode at a time t_1 if the vehicle is too close to the obstacle while the desired course given by the guidance law, denoted $\psi_{f\text{dg}}^n$, is within $\mathcal{V}_{\text{c}}$:

$$\psi_{f\text{dg}}^n(t_1) \in \mathcal{V}_{\text{c}}(t_1), \tag{20a}$$
$$d_{ob}(t_1) \leq d_{\text{switch}}, \tag{20b}$$

where $d_{\text{switch}} > d_{\text{safe}}$ is a design parameter.

Nominal guidance towards the target will resume at a time t_2 when $\psi_{f\text{dg}}^n(t_2)$ moves outside $\mathcal{V}_{\text{c}}(t_2)$,

$$\psi_{f\text{dg}}^n(t_2) \notin \mathcal{V}_{\text{c}}(t_2). \tag{21}$$

To avoid making the vehicle course cross $\mathcal{V}_{\text{c}}$ when approaching $\psi_{f\text{dg}}^n$, we require that $\psi_{f\text{dg}}^n$ is on the same side of $\mathcal{V}_{\text{c}}$ as the vehicle course when exiting collision avoidance:

$$\begin{aligned} j = 1 &: \psi_{f\text{dg}}^n(t_2) - \psi_{f\text{dca}}^{n(1)}(t_2) \leq 0, \\ j = 2 &: \psi_{f\text{dg}}^n(t_2) - \psi_{f\text{dca}}^{n(2)}(t_2) \geq 0. \end{aligned} \tag{22}$$

The angular difference is mapped to the interval

$$\left(\psi_{f\text{dg}}^n(t_2) - \psi_{f\text{dca}}^{n(j)}(t_2)\right) \in (-\pi, \pi], \quad j = \{1, 2\}, \tag{23}$$

which ensures that the vehicle makes the shortest turn towards the desired course.

The switching rule is illustrated in an overtaking scenario in Fig. 4. In Fig. 4(a), the vehicle comes too close to an obstacle on collision course and enters collision avoidance. In Fig. 4(b), the desired course from guidance is outside the vision cone, but the vehicle has to cross $\mathcal{V}_{\text{c}}$ to reach it. Hence, the control system remains in collision avoidance mode. In Fig. 4(c), the desired course from guidance is safe, and the control system enters nominal guidance mode.

C. Turning direction

The proposed CAA algorithm (19) provides two candidate course directions for safe maneuvering, resulting in either a clockwise or counterclockwise collision avoidance maneuver. Both of the candidates are safe, which provides flexibility to consider different scenario preferences or traffic rules. In this paper, we will as an example use a conservative approach,

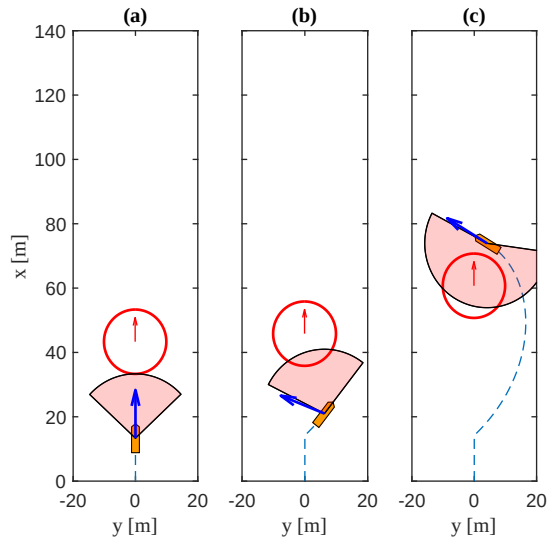

Fig. 4. Illustration of the switching rule. The vehicle (orange) encounters an obstacle (red circle). The compensated vision cone $\mathcal{V}_c$ is drawn in a transparent red, the obstacle velocity is shown as a red arrow and the desired course provided by the guidance law is shown as a blue arrow.

where we make the vehicle move behind the obstacle. Specifically, at a time t_1 at which the control system enters collision avoidance, the turning parameter j is chosen according to:

$$j = \arg\max_{j=1,2} |\psi_o^n(t_1) - \psi_{f\text{dca}}^{n(j)}(t_1)|. \tag{24}$$

The difference between the obstacle course and $\psi_{f\text{dca}}^{n(j)}$ are mapped to the interval $(-\pi, \pi]$. If the obstacle is closer than d_{switch} when the vehicle enters CA mode, the vehicle will make the shortest turn towards a safe direction. Once a turning direction has been chosen, it is kept throughout the collision avoidance maneuver in order to avoid chattering.

Remark 4. *An alternative approach is to choose the turning direction to comply with the International regulations for preventing collisions at sea (COLREGS), as in [19], [24]. The vehicle would then turn to starboard when the obstacle comes from starboard, when the obstacle comes head on, or if the vehicle overtakes the obstacle from behind. If the obstacle approaches from the port side, the vehicle would not yield, i.e. the control system would not enter collision avoidance mode.*

D. Multiple obstacles

The proposed CAA algorithm can be extended to multiple obstacles. While a thorough analysis of a multiobstacle scenario is beyond the scope of this paper, we will in this section present a rule for using the CAA algorithm to safely navigate clusters of obstacles.

We create a compensated vision cone for each obstacle closer to the vehicle than d_{switch}. If any of these cones overlap, they are merged into a single cone. When the control system enters collision avoidance mode, there might thus be more than one obstacle in the current unsafe cone. The closest obstacle is then used to choose the turning direction according to (24).

If a new obstacle joins the cone currently used for avoidance during the maneuver, the cone is extended to include the new obstacle. The vehicle will keep the turning direction, and will follow the corresponding edge of the new vision cone.

Examples of multiobstacle scenarios are presented in the experimental results in Section X.

V. Nominal guidance laws

When the control system is not in collision avoidance mode, it is in nominal guidance mode. In this mode, the vehicle course is steered by a guidance law in order to fulfill the goals of the current scenario. The modular nature of the control system makes it possible to implement a wide array of guidance laws, and in this paper we will present two examples. The first guidance law is for target reaching, which we will achieve using a pure pursuit guidance law, while the second guidance law is a line of sight (LOS) guidance law for path following of straight line paths.

A. Pure pursuit guidance

The pure pursuit (PP) guidance law [29], [30] is a target reaching guidance law which we in this paper will employ to make the vehicle reach a static target position $\boldsymbol{p}_t^n \triangleq [x_t^n, y_t^n]$. To reach the target as soon as possible, we set the desired course to point towards the target position:

$$\psi_{f\text{pp}}^n \triangleq \text{atan2}(y_t^n - y_b^n, x_t^n - x_b^n), \tag{25}$$

where $\psi_{f\text{pp}}^n$ is the desired course during PP guidance.

Remark 5. *If the target was not static, a velocity compensation term like the one computed in* (17) *could be used with the target velocity. The resulting course reference would then make the vehicle reach a slower moving target.*

B. Line of sight guidance

The LOS guidance law for straight line path following was first analyzed in [25], and it was proved in [31] that it provides uniform semiglobal exponential stability when applied to an underactuated marine vehicle as the one modeled in (6).

The guidance law is illustrated in Fig. 5. The idea is to mimic the way an experienced helmsman steers a vehicle by aiming the vehicle course towards a point ahead of it on the path. Specifically, the target point lies a lookahead distance Δ meters ahead of the vehicle along the path, where Δ is a positive control parameter.

If we, for conciseness and without loss of generality, assume that the path $\mathcal{P}$ is oriented along the x-axis of the NED frame,

$$\mathcal{P} \triangleq \{(x^n, y^n) \in \mathbb{R}^2 : y^n = 0\}, \tag{26}$$

then the guidance law is defined as

$$\psi_{f\text{los}}^n \triangleq \text{atan2}(-y_b^n, \Delta), \tag{27}$$

where $\psi_{f\text{los}}^n$ is the desired course during LOS guidance.

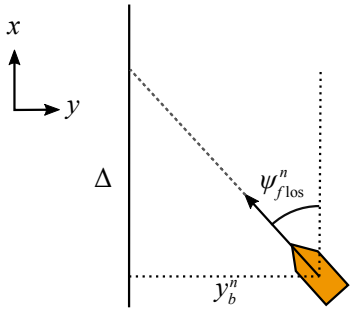

Fig. 5. Illustration of the LOS guidance law steering the orange vehicle onto the path $\mathcal{P}$, which is drawn as a solid black line.

VI. Course controller

In this section we will present the course controller used to follow the references from either the CAA guidance law or from a nominal guidance law. The course controller gives references to the yaw rate controller presented in Section VII, and is implemented as a proportional controller. To limit the turning rate, and hence the induced sway motion, the proportional effect is saturated. The controller is defined as:

$$r_{fd} \triangleq \dot{\psi}^n_{fd} - \text{sat}(k_f \tilde{\psi}^n_f), \tag{28}$$

where r_{fd} is the desired yaw rate signal, the course error is denoted $\tilde{\psi}^n_f \triangleq \psi^n_{fd} - \psi^n_f \in (-\pi, \pi]$, the control gain k_f is a positive design parameter, and ψ^n_{fd} is the course reference from either one of the nominal guidance laws presented in Section V, or from the CAA collision avoidance law of Section IV. The saturation function $\text{sat}(k_f \tilde{\psi}^n_f)$ is defined as

$$\text{sat}(k_f \tilde{\psi}^n_f) \triangleq \begin{cases} r_{fp}, & k_f \tilde{\psi}^n_f > r_{fp}, \\ k_f \tilde{\psi}^n_f, & k_f \tilde{\psi}^n_f \in [-r_{fp}, r_{fp}], \\ -r_{fp}, & k_f \tilde{\psi}^n_f < -r_{fp}, \end{cases} \tag{29}$$

where the parameter $r_{fp} > 0$ is a constant design parameter. In order to ensure that the saturation is in effect on an error in the interval $\tilde{\psi}^n_f \in (-\pi, \pi]$, we make the following assumption on r_{fp}:

Assumption 8.

$$r_{fp} \leq k_f \pi. \tag{30}$$

A yaw rate reference signal $\bar{r}_{bd}$ is then created by solving (9) for r_b:

$$\bar{r}_{bd} \triangleq \frac{U_b^2 r_{fd} - Y(u_b) u_b v_b + \dot{u}_b v_b}{X(u_b) u_b + U_b^2}. \tag{31}$$

This signal is ensured to be well defined by Assumption 5. Note that, when the control system switches mode, there is a discontinuity in $\bar{r}_{bd}$. To avoid this, we will in the next section introduce a bump function to ensure that the yaw rate signal is always continuous.

A. Yaw rate bump function

To avoid discontinuities in the desired yaw rate, we introduce a linear bump function $\delta(t_d)$:

$$\delta(t_d) = \begin{cases} 1, & t_d \geq t_\delta, \\ \frac{t_d}{t_\delta}, & 0 < t_d < t_\delta \\ 0, & t_d \leq 0, \end{cases} \tag{32}$$

where the bump time t_δ is a positive constant.

As long as the yaw rate signal $\bar{r}_{bd}$ from (31) is smooth, $r_{bd} = \bar{r}_{bd}$. However, if there is a jump in $\bar{r}_{bd}$ at time t_1, we apply the bump function:

$$r_{bd}(t) = r_{bd}(t_1)\left[1 - \delta(t - t_1)\right] + \bar{r}_{bd}(t)\delta(t - t_1). \tag{33}$$

This ensures that when $t \geq t_1 + t_\delta$, $r_{bd}(t) = \bar{r}_{bd}(t)$. If, at a time $t_2 \in (t_1, t_1 + t_\delta)$, $r_{bd}(t_2) = \bar{r}_{bd}(t_2)$, use of the smoothing function is stopped until the next discontinuity in $\bar{r}_{bd}$.

VII. Surge and yaw rate controllers

The surge (6d) and yaw rate (6f) are controlled using feedback linearizing controllers like the one described in [33]:

$$\tau_u = -F_{u_b}(u_b, v_b, r_b) + \dot{u}_{bd} - k_u(\tilde{u}_b), \tag{34a}$$
$$\tau_r = -F_{r_b}(u_b, v_b, r_b) + \dot{r}_{bd} - k_r(\tilde{r}_b), \tag{34b}$$

where $k_u > 0$ and $k_r > 0$ are constant control gains, and $\tilde{u}_b \triangleq u_b - u_{bd}$ and $\tilde{r}_b \triangleq r_b - r_{bd}$.

Inserting these controllers into (6d) and (6f) gives the following error dynamics:

$$\dot{\tilde{u}}_b = -k_u \tilde{u}_b, \tag{35a}$$
$$\dot{\tilde{r}}_b = -k_r \tilde{r}_b. \tag{35b}$$

The error dynamics are linear, and globally exponentially stable at the origin. Hence, as long as r_{bd} and u_{bd} are continuous signals, a vehicle described by (6) will be able to follow them as long as the following assumption is met:

Assumption 9. *At time t_0, the system has operated long enough for the surge and yaw rate to converge, i.e. $\tilde{u}_b(t_0) = 0$ and $\tilde{r}_b(t_0) = 0$.*

Remark 6. *To fulfill this assumption, the vehicle needs to be properly initialized before control is handed over to the automatic collision avoidance system, which is reasonable.*

Remark 7. *We have assumed that the vehicle is able to follow the surge speed reference during the maneuver. However, if there is a perturbation in the vehicle surge, the CAA algorithm will compensate the desired course according to the actual surge speed, as seen in* (17)*. Thus, the output from the algorithm remains safe.*

VIII. Mathematical analysis

This section contains a mathematical analysis of the system in collision avoidance mode. For this section, we make the following assumption:

Assumption 10. *The distance between two obstacles are always at least $2d_{switch}$.*

Dette er en postprint-versjon/This is a postprint version. Publisert versjon/Publised version: https://doi.org/10.1109/TCST.2019.2903451

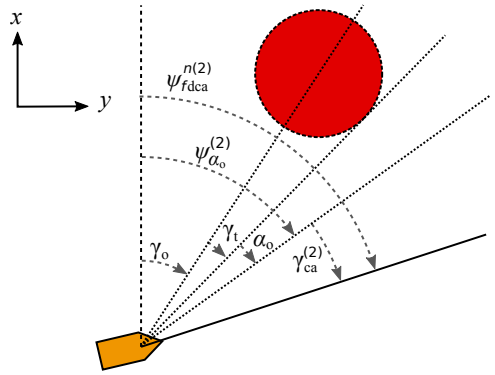

Fig. 6. Decomposition of the angle $\psi^{n(2)}_{f\text{dca}}$.

This assumption ensures that the vehicle will only have to avoid one obstacle at a time.

A. Minimum obstacle distance

We start by finding a lower bound on the distance to the obstacle the vehicle will reach when following the CAA guidance law around a static obstacle.

Lemma 1. *Let the obstacle velocity be zero, and let the avoidance angle be in the interval $\alpha_o \in (0, \frac{\pi}{2})$. Furthermore, let the vehicle follow the course reference from the CAA collision avoidance law* (19) *when $t \geq t_1$, with some speed $U_b > 0$. If $d_{ob}(t_1) \geq 0$, the vehicle will converge to a circle $\mathcal{C}$ with center at the obstacle center and radius $R_c = \frac{R_o}{\cos(\alpha_o)}$. Furthermore, if the vehicle starts outside $\mathcal{C}$, then*

$$d_{ob}(t) \geq d_{\min} \triangleq \frac{R_o}{\cos(\alpha_o)} - R_o, \quad \forall t \geq t_1. \tag{36}$$

Proof. The course reference $\psi^{n(j)}_{f\text{dca}}$ keeps a constant avoidance angle α_o to one of the tangents from the vehicle to the obstacle, as shown in Fig. 2. The time derivative of d_{ob} can then be found geometrically as

$$\dot{d}_{ob} = -U_b \cos(\gamma_\text{t} + \alpha_\text{o}), \tag{37}$$

where γ_t is the angle from the line connecting the vehicle and the center of the obstacle to the tangent line as seen in Fig. 6:

$$\gamma_\text{t} \triangleq \sin^{-1}\left(\frac{R_o}{R_o + d_{ob}}\right), \quad d_{ob} \geq 0. \tag{38}$$

When $d_{ob} > d_{\min}$, we obtain $\gamma_\text{t} + \alpha_0 < \frac{\pi}{2}$, which gives $\dot{d}_{ob} < 0$. Similarly, when $d_{ob} < d_{\min}$, $\dot{d}_{ob} > 0$. Finally, when $d_{ob} = d_{\min}$, $\dot{d}_{ob} = 0$. Hence, the vehicle will converge to $\mathcal{C}$, and if $d_{ob}(t_1) > d_{\min}$ then $d_{ob}(t) \geq d_{\min}$ $\forall t \geq t_0$. □

The proof of Lemma 1 is illustrated in Fig. 7.

B. Upper bound on the vehicle sway

During the collision avoidance maneuver, the switching distance and the required course rate of the vehicle will depend on the vehicle's speed $U_b = \sqrt{u_b^2 + v_b^2}$. To find an upper bound on the U_b, we need to find an upper bound on the sway movement v_b. This is done in the following Lemma, which uses the sway dynamics in (10).

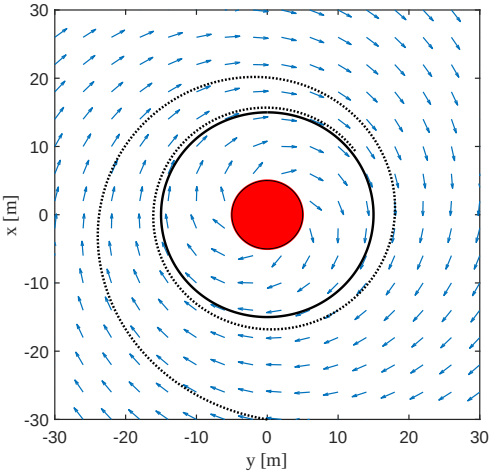

Fig. 7. A vector field showing the desired vehicle course when the turning direction $j = 1$. The red circle is the obstacle, the black circle represents $d_{\min}$ and the dotted black line shows an example integral curve of the field.

Lemma 2. *Let the vehicle be modeled by* (6)*, and let Assumptions 4-6 and 9 hold. Suppose that r_{fd} depends on the vehicle sway speed v_b, and that for $v_{b,\text{sup}} > 0$,*

$$|r_{fd}(v_{b,\text{sup}})| < \frac{|Y_d|}{|X_d|} v_{b,\text{sup}}. \tag{39}$$

Finally, let $v_b(t_0) < v_{b,\text{sup}}$. Then,

$$v_b(t) < v_{b,\text{sup}} \quad \forall t \geq t_0. \tag{40}$$

Proof. Consider the Lyapunov function candidate $V(v_b) = 0.5 v_b^2$ of (10). The time derivative of V along the solutions of (10) is

$$\dot{V} = \frac{U_b^2 v_b}{U_b^2 + X_\text{d} u_{b\text{d}}} \left(X_\text{d} r_{f\text{d}} + Y_\text{d} v_b\right). \tag{41}$$

When Assumption 4 holds, (41) is bounded by

$$\dot{V} \leq \frac{U_b^2 |v_b|}{U_b^2 + X_\text{d} u_{b\text{d}}} \left(|X_\text{d}||r_{f\text{d}}(v_b)| - |Y_\text{d}||v_b|\right). \tag{42}$$

Let the set Ω_v be defined as

$$\Omega_v \triangleq \{v_b \in \mathbb{R} \mid V \leq \tfrac{1}{2} v_{b,\text{sup}}^2\}, \tag{43}$$

which is a level set of V with $v_b = v_{b,\text{sup}}$ on the boundary. Equation (39) ensures that $\dot{V} \leq 0$ on the boundary of Ω_v. Hence, Ω_v is positively invariant and it follows that any solution of v_b starting in the set Ω_v cannot leave it. Hence, if $|v_b(t_0)| < v_{b,\text{sup}}$, then $|v_b(t)| < v_{b,\text{sup}}$ $\forall t \geq t_0$. □

We will treat $v_{b,\text{sup}}$ as a design parameter in the remainder of the paper. This parameter is in the next section used to find bounds on the minimum safety distance d_safe and on the course control proportional saturation r_{fp}, and can be used to adjust the aggressiveness of the collision avoidance maneuver to satisfy both scenario preferences and actuator constraints.

C. Bounds on safety distance and course control

Before stating the next lemma, we define the following term for conciseness:

$$F_{\text{kd}} \triangleq |Y_{\text{d}}| v_{b,\sup} \left(\frac{1}{|X_{\text{d}}|} - 2 \frac{v_{b,\sup} u_o}{U_{\text{d,sup}} \left(X_{\text{d}} u_{b\text{d}} + U_{b,\sup}^2 \right)} \right), \tag{44}$$

where $U_{b,\sup} \triangleq \sqrt{u_{b\text{d}}^2 + v_{b,\sup}^2}$ and $U_{\text{d,sup}} \triangleq \sqrt{U_{b,\sup}^2 - u_o^2}$.

We also introduce the design parameter $\sigma \in (0,1)$, which is used to prioritize between the course control proportional saturation r_{fp} and the safety distance d_{safe}. A high value of σ will give priority to a high r_{fp}, which will enable the vehicle to turn faster, while a low value of σ prioritizes a low d_{safe}, which will require a higher turning rate as the vehicle will maneuver closer to the obstacle.

Lemma 3. *Consider a vehicle modeled by* (6)*. Let the vehicle be governed by the surge and yaw rate controllers* (34) *and the course controller* (28)*. Let the control system enter collision avoidance mode at time t_1, and let the course then be guided by the CAA algorithm* (19)*. Furthermore, assume that the vehicle course satisfies $\psi_f^n(t_2) = \psi_{fdca}^{n(j)}(t_2)$ at some time $t_2 \geq t_1 + t_d$. Finally, let $\sigma \in (0,1)$, and assume that the distance between the vehicle and the obstacle satisfies $d_{ob}(t) > d_{safe}$ $\forall t \geq t_1$. If Assumptions 1-10 hold, the course control proportional saturation r_{fp} satisfies*

$$r_{fp} \leq \sigma F_{kd}, \tag{45}$$

the safety distance d_{safe} satisfies

$$d_{safe} \geq \frac{\left(U_{b,\sup} + u_{o,\max}\right)^2}{U_{b,\sup}} \frac{1}{(1-\sigma) F_{kd}}, \tag{46}$$

and the sway speed satisfies $|v_b(t_0)| < v_{b,\sup}$, then

$$|v_b(t)| < v_{b,\sup} \quad \forall t \geq t_0 \tag{47}$$

Proof. Lemma 3 is proved by finding an upper bound on $r_{f\text{d}}$ for a given $v_{b,\sup}$. The upper bound is inserted into (39), which allows us to apply Lemma 2. We then obtain (45) and (46) by solving for r_{fp} and d_{safe}.

The time derivative of $\psi_{f\text{dca}}^{n(j)}$ is

$$\dot{\psi}_{f\text{dca}}^{n(j)} = \dot{\psi}_{\alpha_{\text{o}}}^{(j)} + \dot{\gamma}_{\text{ca}}^{(j)}. \tag{48}$$

The time derivative of $\gamma_{\text{ca}}^{(j)}$ is found from (17) as

$$\dot{\gamma}_{\text{ca}}^{(j)} = \frac{u_o \left(U_b \dot{\psi}_{\alpha_{\text{o}}}^{(j)} \cos(\gamma_{vo}^{(j)}) - \dot{U}_b \sin(\gamma_{vo}^{(j)}) \right)}{U_b \sqrt{U_b^2 - u_o^2 \sin^2(\gamma_{vo}^{(j)})}}. \tag{49}$$

As shown in Fig. 6, the angle $\psi_{\alpha_{\text{o}}}^{(j)}$ can be decomposed into

$$\psi_{\alpha_{\text{o}}}^{(j)} = \gamma_{\text{o}} \pm \gamma_{\text{t}} \pm \alpha_{\text{o}}. \tag{50}$$

Hence,

$$\dot{\psi}_{\alpha_{\text{o}}}^{(j)} = \dot{\gamma}_{\text{o}} \pm \dot{\gamma}_{\text{t}}. \tag{51}$$

The angular rate $\dot{\gamma}_{\text{o}}$ can be found geometrically as

$$\dot{\gamma}_{\text{o}} = \frac{u_o \sin(\psi_o^n - \gamma_{\text{o}}) - U_b \sin(\psi_f^n - \gamma_{\text{o}})}{R_o + d_{ob}}. \tag{52}$$

while $\dot{\gamma}_{\text{t}}$ is found as

$$\dot{\gamma}_{\text{t}} = -\dot{d}_{ob} \frac{R_o}{(R_o + d_{ob}) \sqrt{(R_o + d_{ob})^2 - R_o^2}}, \tag{53}$$

where

$$\dot{d}_{ob} = u_o \cos(\psi_o^n - \gamma_{\text{o}}) - U_b \cos(\psi_f^n - \gamma_{\text{o}}). \tag{54}$$

Combining (52) - (54) gives

$$\begin{aligned} \dot{\psi}_{\alpha_{\text{o}}}^{(j)} = & \frac{U_b \sin(\gamma_{\text{o}} - \psi_f^n) - u_o \sin(\gamma_{\text{o}} - \psi_o^n)}{R_o + d_{ob}} \\ & \mp R_o \frac{U_b \cos(\gamma_{\text{o}} - \psi_f^n) - u_o \cos(\gamma_{\text{o}} - \psi_o^n)}{(R_o + d_{ob}) \sqrt{d_{ob}\,(2R_o + d_{ob})}}. \end{aligned} \tag{55}$$

The total vehicle acceleration $\dot{U}_b$ is found as

$$\dot{U}_b = U_b v_b \frac{X_{\text{d}} r_{f\text{d}} + Y_{\text{d}} v_b}{X_{\text{d}} u_{b\text{d}} + U_b^2}, \tag{56}$$

where we have used the fact that $\dot{u}_b = \dot{u}_{b\text{d}} = 0$ by Assumption 6. Note that $\dot{\psi}_{f\text{dca}}^{n(j)}$ depends on $r_{f\text{d}}$, which again depends on $\dot{\psi}_{f\text{dca}}^{n(j)}$ when the control system is in collision avoidance mode. A closed expression for $r_{f\text{d}}$ is found by inserting (48) into the course control law (28), which gives

$$r_{f\text{d}} = \frac{F_{\text{num}}}{F_{\text{den}}}, \tag{57}$$

where

$$\begin{aligned} F_{\text{num}} \triangleq & \dot{\psi}_{\alpha_{\text{o}}}^{(j)} + \frac{1}{\sqrt{U_b^2 - u_o^2 \sin^2(\gamma_{vo}^{(j)})}} \\ & \cdot \left[\sin(\gamma_{vo}^{(j)}) \left(\dot{u}_o - \frac{u_o Y_{\text{d}} v_b^2}{U_b^2 + X_{\text{d}} u_{b\text{d}}} \right) + \right. \\ & \left. u_o \cos(\gamma_{vo}^{(j)}) \left(\dot{\psi}_{\alpha_{\text{o}}}^{(j)} - \dot{\psi}_o^n \right) \right] - \text{sat}(k_f \tilde{\psi}_f^n), \end{aligned} \tag{58}$$

and

$$F_{\text{den}} \triangleq 1 + \frac{u_o \sin(\gamma_{vo}^{(j)}) v_b X_{\text{d}}}{(U_b^2 + X_{\text{d}} u_{b\text{d}}) \sqrt{U_b^2 - u_o^2 \sin^2(\gamma_{vo}^{(j)})}}. \tag{59}$$

The expression for (59) is ensured to be well defined by Assumptions 5 and 7. However, in order to ensure that $r_{f\text{d}}$ (57) is well defined, we require that $F_{\text{den}} > 0$. We obtain a lower bound on (59) by minimizing with respect to $\gamma_{vo}^{(j)}$ and v_b:

$$F_{\text{den}} > 1 - \frac{u_{o,\max} |v_b| |X_{\text{d}}|}{(U_b^2 + X_{\text{d}} u_{b\text{d}}) \sqrt{U_b^2 - u_{o,\max}^2}} := F_{\text{den,inf}}(v_b). \tag{60}$$

Minimizing (60) with respect to v_b and solving for $u_{o,\max}$ gives the following bound on $u_{o,\max}$ to ensure that $F_{\text{den}} > 0$ for all $u_o \in [0, u_{o,\max}]$:

$$u_{o,\max} < \begin{cases} 2\sqrt{-X_{\text{d}}^2 - X_{\text{d}} u_{b\text{d}}} & -u_{b\text{d}} < X_{\text{d}} \leq -\frac{u_{b\text{d}}}{2} \\ u_{b\text{d}} & -\frac{u_{b\text{d}}}{2} < X_{\text{d}}. \end{cases} \tag{61}$$

Assumption 7 ensures that (61) is satisfied.

When $d_{ob} \geq d_{\text{safe}}$, a bound $|F_{\text{num}}| < F_{\text{num,sup}}$ can be found by using Assumptions 4 and 6-9, where:

$$F_{\text{num,sup}} \triangleq \frac{v_{b,\sup}^2 |Y_{\text{d}}| u_o}{U_{\text{d,sup}} \left(X_{\text{d}} + U_{b,\sup}^2 \right)} + \frac{\left(U_{b,\sup} + u_o \right)^2}{d_{\text{safe}} U_{b,\sup}} + r_{fp}. \tag{62}$$

Equations (60) and (62) are even in v_b and $v_{b,\sup}$, respectively. Hence,

$$|r_{fd}(\pm v_{b,\sup})| < \frac{F_{\text{num,sup}}}{F_{\text{den,inf}}(v_{b,\sup})}. \tag{63}$$

Inserting (63) into (39) bounds d_{safe} and r_{fp} to:

$$\frac{(U_{b,\sup}+u_{o,\max})^2}{d_{\text{safe}}U_{b,\sup}} + r_{fp} \leq F_{\text{kd}}, \tag{64}$$

where F_{kd} is given in (44). The design parameter σ can be used to rewrite (64) as

$$\frac{(U_{b,\sup}+u_{o,\max})^2}{d_{\text{safe}}U_{b,\sup}} + r_{fp} \leq \sigma F_{\text{kd}} + (1-\sigma)F_{\text{kd}}. \tag{65}$$

Hence, conditions (45) and (46) ensure that (64) is satisfied. Condition (39) of Lemma 2 then also applies, and it follows that if $|v_b(t_0)| < v_{b,\sup}$, then $|v_b(t)| < v_{b,\sup}\ \forall t \geq t_0$. □

D. Minimum switching distance

We will now provide a lower bound on the switching distance in order to ensure that the vehicle course angle is within ϵ radians of the desired course from the CAA algorithm before the obstacle can get too close to the vehicle.

Lemma 4. *Let a vehicle be modeled by* (6)*, and let it be controlled by the feedback linearizing controllers* (34) *and the course controller* (28)*. At a time $t_1 \geq t_0$, let the control system enter collision avoidance mode according to the switching rule in Section IV-B, and let the vehicle course then be set by the collision avoidance law* (19)*. Furthermore, let Assumptions 1-7 be satisfied, the vehicle speed satisfy $U_b < U_{b,\sup}$, and the switching distance satisfy*

$$d_{switch} \geq u_o t_\epsilon + d_{safe} + d_{turn} + d_\delta, \tag{66}$$

where

$$t_\epsilon \triangleq t_\delta + \left(\frac{\pi}{r_{fp}} - \frac{1}{k_f}\right) - \frac{\ln(k_f\epsilon/r_{fp})}{k_f}, \quad \epsilon \in (0, \tilde{\psi}^n_{fp}] \tag{67}$$

is the maximum amount of time the course controller (28) *will use to make the vehicle converge to within ϵ rad of $\psi^{n(j)}_{fdca}$, and*

$$d_{turn} \triangleq \frac{U_{b,\sup}}{\min(r_{fp}, k_f\frac{\pi}{2})} \tag{68}$$

upper bounds the distance traveled by the vehicle in the $\psi^n_f(t_1)$ direction when making a complete π rad turn. The distance d_δ is

$$d_\delta \triangleq U_{b,\sup} t_\delta. \tag{69}$$

Then, the vehicle is able to converge to within ϵ rad of $\psi^{n(j)}_{fdca}$ before the obstacle can come within the distance d_{safe}.

Proof. The main idea behind the proof is to show that the distance traveled by the obstacle during the convergence time t_ϵ is not enough to reduce the distance between the obstacle and the vehicle trajectory as it turns away from the obstacle to less than d_{safe}. This is illustrated in Fig. 8.

We consider a worst case scenario with an obstacle of infinite size, $R_o \to \infty$. The obstacle tangent angle is then $\gamma_{\text{t}} = \pi/2$. Furthermore, the vehicle and obstacle move at maximum speed, i.e. $U_b(t_1) = U_{b,\sup}$ and $u_o(t_1) = u_{o,\max}$. We assume, without loss of generality, that the obstacle is ahead of the vehicle on the x-axis of the NED frame, $x^n_o(t_1) - x^n_b(t_1) = d_{\text{switch}}$, while $y^n_o(t_1) = x^n_o(t_1) = 0$, and that they move straight towards each other, $\psi^n_f(t_1) = 0$ and $\psi^n_o(t_1) = \pi$. The worst case behavior of the obstacle is then to continue moving straight towards the vehicle at maximum speed, $u_o(t > t_1) = u_{o,\max}$ and $\psi^n_o(t > t_1) = \pi$.

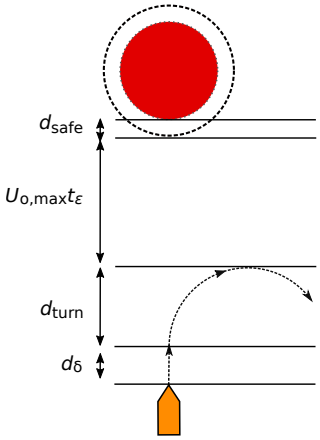

Fig. 8. Illustration of the minimum required switching distance.

At time t_1, when the control system enters collision avoidance mode, the vehicle starts to make a turn towards $\psi^{n(j)}_{f\text{dca}}$. There will then be a jump in the desired yaw rate from the course controller, and the yaw rate smoothing (33) will commence. The smoothing is complete at time $t_1 + t_\delta$. Since $\tilde{\psi}^n_f \in (-\pi, \pi]$, the maximum course error at time $t = t_1 + t_\delta$ is π radians. The convergence time from $|\tilde{\psi}^n_f| = \pi$ to $|\tilde{\psi}^n_f| = r_{fp}/k_f$ is found from (28) to be $\pi/r_{fp} - 1/k_f$, which is ensured to be positive from Assumption 8. From this point, the course converges exponentially, and hence the convergence time from $|\tilde{\psi}^n_f| = r_{fp}/k_f$ to $|\tilde{\psi}^n_f| < \epsilon$ is $\frac{\ln(k_f\epsilon/r_{fp})}{k_f}$.

It follows that the total time from t_1 until $|\tilde{\psi}^n_f| \leq \epsilon$ is t_ϵ as defined in (67). During this time, the obstacle will, at worst, have traversed $u_{o,\max}t_\epsilon$ towards the vehicle.

During the smoothing interval $t \in (t_1, t_1 + t_\delta]$, the distance covered by the vehicle towards the obstacle is upper bounded by d_δ. During the first $\pi/2$ radians of the following turn, the vehicle will move towards the obstacle. We see from geometry that the compensated vision cone $\mathcal{V}_{\text{c}}$ will then expand. Hence, $\psi^{n(j)}_{f\text{dca}}$ will move away from ψ^n_f during this part of the turn, and the turning rate of the vehicle can be lower bounded by setting $\dot{\psi}^n_{f\text{d}} = 0$ in the course controller. In a worst case scenario, the vehicle has to turn completely around. Assumption 8 then ensures that the vehicle will move at most d_{turn} towards the obstacle when turning.

Hence, if condition (66) holds, then the distance between the obstacle and the vehicle trajectory will not be reduced to less than d_{safe} before the vehicle course has converged to within ϵ rad of $\psi^{n(j)}_{f\text{dca}}$. It follows that the obstacle is thus more than d_{safe} meters from the vehicle, which concludes the proof. □

We are now ready to state the main theorems of the paper,

namely safe maneuvering both in a target reaching and in a path following scenario. Before we state these theorems, we need to assume that the vehicle starts safely:

Assumption 11.

$$d_{ob}(t_0) > d_{switch}. \tag{70}$$

Remark 8. *Like Assumption 9, this assumption corresponds to assuming that the vehicle is safely initialized before control is handed over to the automatic collision avoidance system.*

E. Safe target reaching

In this section, we will provide conditions to ensure that the CAA collision avoidance algorithm (19) in combination with the pure pursuit guidance law (25) enables the vehicle to safely maneuver to the target. In order to do this, we must assume that the distance from the target to the obstacle is greater than the minimum obstacle distance:

Assumption 12. *The distance $d_{ot}(t)$ from the target to the obstacle satisfies*

$$d_{ot}(t) > \frac{R_o}{\cos(\alpha_o)} - R_o \quad \forall t \geq t_0. \tag{71}$$

Theorem 1. *Let Assumptions 1-12 hold, the avoidance angle satisfy*

$$\alpha_o \in \left[\cos^{-1}\left(\frac{R_o}{R_o + d_{safe}}\right) + \epsilon, \frac{\pi}{2}\right) \tag{72}$$

and the switching distance satisfy

$$d_{switch} \geq u_{o,\max} t_\epsilon + d_{safe} + d_{turn} + d_\delta, \tag{73}$$

where t_ϵ, d_{turn} and d_δ are defined in Lemma 4. Furthermore, let the course control proportional saturation level r_{fp} and the safety distance d_{safe} satisfy the conditions of Lemma 3:

$$r_{fp} \leq \sigma F_{kd}, \tag{74}$$

$$d_{safe} \geq \frac{(U_{b,\sup} + u_{o,\max})^2}{U_{b,\sup}} \frac{1}{(1-\sigma)F_{kd}}. \tag{75}$$

Finally, let the initial vehicle sway satisfy $|v_b(t_0)| < v_{b,\sup}$.

Then, a vehicle described by (6)*, controlled by the surge and yaw rate controllers* (34)*, the course controller* (28)*, the pure pursuit guidance law* (25) *and the CAA collision avoidance law* (19) *will maneuver to the target position $\boldsymbol{p}_t$ in the presence of an obstacle described by* (12) *while ensuring that*

$$d_{ob}(t) \geq d_{safe} > 0 \quad \forall t \in [t_0, t_f], \tag{76}$$

where t_f is the time of arrival at $\boldsymbol{p}_t$.

Proof. It follows from Lemma 3 that v is bounded by

$$|v_b(t)| < v_{b,\sup} \quad \forall t \in [t_0, t_f]. \tag{77}$$

Hence, the vehicle speed is bounded by $U_b < U_{b,\sup}$. Denote the time when (20) is fulfilled by $t_1 \geq t_0$. At this time, the control system enters collision avoidance mode as described in Section IV-B. Lemma 4 then ensures that there is a time $t_2 > t_1$ when $d(t_1) >= d_{\text{safe}}$ and $\psi_f^n(t_2) - \psi_{f\text{dca}}^n(t_2) \leq \epsilon$. Since the yaw rate reference signal r_{bd} is smooth by (33), the vehicle course has a locally exponentially stable equilibrium at $\tilde{\psi}_f^n = 0$ when the course controller (28) is employed. Hence, it is ensured that

$$\psi_f^n(t) - \psi_{f\text{dca}}^{n(j)}(t) \leq \epsilon, \quad \forall t \in [t_2, t_3], \tag{78}$$

where t_3 is the time when the control system will exit collision avoidance mode.

In a coordinate frame O moving with the obstacle velocity $\dot{\boldsymbol{p}}_o^n$, the vehicle velocity is within ϵ radians of $\boldsymbol{v}_{\alpha_o}^{(j)}(t)$, defined in (14). Assumption 7 ensures that $u_{\alpha_o} > 0$. Hence, Lemma 1 ensures that

$$d_{ob}(t) \geq d_{\text{safe}} \quad \forall t \in [t_2, t_3], \tag{79}$$

which satisfies condition (76).

Since the vehicle circles the obstacle, there will be a time t_3 when the direction to the target will be outside of $\mathcal{V}_c$. The vehicle will then exit collision avoidance mode and proceed towards the target. □

F. Safe path following

In this section, we will provide conditions to ensure that the CAA collision avoidance algorithm (19) in combination with the line of sight guidance law (27) enables the vehicle to safely maneuver around the obstacle and reach the path.

Theorem 2. *Let Assumptions 1-11 hold, the avoidance angle satisfy*

$$\alpha_o \in \left[\cos^{-1}\left(\frac{R_o}{R_o + d_{safe}}\right) + \epsilon, \frac{\pi}{2}\right) \tag{80}$$

and the switching distance satisfy

$$d_{switch} \geq u_{o,\max} t_\epsilon + d_{safe} + d_{turn} + d_\delta, \tag{81}$$

where t_ϵ, d_{turn} and d_δ are defined in Lemma 4. Furthermore, let the course control proportional saturation level r_{fp} and the safety distance d_{safe} satisfy the conditions of Lemma 3:

$$r_{fp} \leq \sigma F_{kd}, \tag{82}$$

$$d_{safe} \geq \frac{(U_{b,\sup} + u_{o,\max})^2}{U_{b,\sup}} \frac{1}{(1-\sigma)F_{kd}}. \tag{83}$$

Finally, let the initial vehicle sway satisfy $|v_b(t_0)| < v_{b,\sup}$ and the lookahead distance Δ satisfy

$$\Delta \geq \frac{U_{b,\sup}|X_d|}{(|Y|v_{b,\sup} - |X|r_{fp})}. \tag{84}$$

Then, a vehicle described by (6)*, controlled by the surge and yaw rate controllers* (34)*, the course controller* (28)*, the line of sight guidance law* (27) *and the CAA collision avoidance law* (19) *will converge to and follow a path $\mathcal{P}$ given by* (26) *until it encounters an obstacle modeled by* (12)*. The obstacle will be safely avoided, and the vehicle will converge to the path again after the collision avoidance maneuver. Furthermore, it is ensured that*

$$d_{ob}(t) \geq d_{safe} > 0 \quad \forall t \geq t_0. \tag{85}$$

Proof. The required turning rate of the LOS guidance law is found as

$$\dot{\psi}_{f\text{los}}^n = -\frac{\Delta \dot{y}_b^n}{\Delta^2 + y_b^{n\,2}}, \tag{86}$$

which is bounded as

$$|\dot{\psi}^n_{f\text{los}}| \leq \frac{U_{b,\text{sup}}}{\Delta}. \tag{87}$$

Inserting (87) into the course controller (28) gives a maximum desired course rate of

$$|r_{f\text{los}}| \leq \frac{U_{b,\text{sup}}}{\Delta} + r_{fp}. \tag{88}$$

Applying Lemma 2 on (88) gives that if

$$\Delta \geq \frac{U_{b,\text{sup}}|X_\text{d}|}{(|Y|v_{b,\text{sup}} - |X|r_{fp})}, \tag{89}$$

and $|v_b(t_0)| < v_{b,\text{sup}}$, then $|v_b(t)| < v_{b,\text{sup}}$ until a time t_2 when the vehicle enters collision avoidance mode. Along with Lemma 3, we then obtain that

$$|v_b(t)| < v_{b,\text{sup}} \quad \forall t \in [t_0, t_f]. \tag{90}$$

The rest of the proof is equivalent to the proof of Theorem 1. □

IX. Simulation Results

In this section we present numerical simulations of an underactuated marine vehicle using the proposed collision avoidance algorithm. The simulated vehicle is a HUGIN autonomous underwater vehicle [34] operating in a horizontal plane. The desired vehicle surge speed is set to $u_{bd} = 2\,\text{m/s}$, and the maximum allowable sway speed is set to $v_{b,\text{sup}} = 2\,\text{m/s}$. It can be verified that Assumption 4 is satisfied with $Y_\text{d} = -1.10$, and that Assumption 5 is satisfied with $X_\text{d} = -1.59$. The initial sway velocity was zero in all simulations, while $u_b(t_0) = 2\,\text{m/s}$ and $\psi^n_b(t_0) = 0\,\text{rad}$.

In the three first scenarios the vehicle encounters an obstacle head on, from the starboard side and from the port side, respectively. These scenarios all contain a circular obstacle with radius $R_o = 15\,\text{m}$. The obstacle speed is $u_o = 1\,\text{m/s}$, which satisfies Assumption 7. The course control proportional saturation level r_{fp} is set to $0.17\,\text{rad/s}$, and the safety distance is set to $d_\text{safe} = 10\,\text{m}$, which satisfies the conditions of Lemma 3 with $\sigma = 0.25$. The course control gain k_f is set to $0.4\,\text{s}^{-1}$, satisfying (30), while the convergence parameter ϵ is set to $\epsilon = 0.05\,\text{rad}$. The switching distance d_switch is set to $70\,\text{m}$, while α_o is set to $0.97\,\text{rad}$, satisfying (46) and (72).

The first scenario is illustrated in Fig. 9. The vehicle steers towards a target position using the pure pursuit guidance law (25). The obstacle starts in front of the vehicle on a head on collision course. At time $8.35\,\text{s}$ the vehicle reaches the switching distance d_switch from the obstacle, and enters collision avoidance mode in accordance with the switching rule in Section IV-B. Since the vehicle and the obstacle are on a head on collision course, the choice of turning direction given in Section IV-C becomes random. In this case, the vehicle makes a port turn. The vehicle maneuvers safely around the obstacle until time $42.85\,\text{s}$, when the direction towards the target comes outside of the unsafe cone. The vehicle then proceeds towards the target in accordance with Theorem 1.

In the second scenario, which is shown in Fig. 10, the obstacle crosses from starboard. The pure pursuit guidance law is again employed to take the vehicle towards the target position. When the control system enters collision avoidance mode at time $1.44\,\text{s}$, the vehicle turns starboard to maneuver behind the obstacle. At time $43.58\,\text{s}$, the direction to the target is safe and the vehicle proceeds towards it.

The collision avoidance algorithm in combination with the LOS guidance law (27) is demonstrated in the third scenario, which is shown in Fig. 11. The obstacle now approaches in front of the vehicle from the port side, while the vehicle follows a straight line path along the x^n-axis. At time $6.47\,\text{s}$ the desired course from the LOS guidance law, $\psi^n_{f\text{los}}$, comes within $\mathcal{V}_\text{c}$, and the control system enters collision avoidance mode. The vehicle maneuvers safely behind the obstacle, until

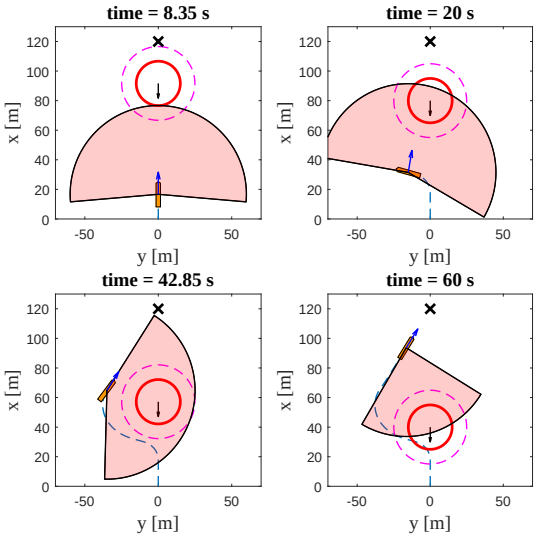

Fig. 9. The vehicle meets an obstacle head on in the first scenario. The vehicle is shown in orange, while the obstacle is a solid red circle. A dotted red circle shows d_safe, while $\mathcal{V}_\text{c}$ is shown as a semi-opaque red sector of radius d_switch. The target position is marked by an 'X', and the blue arrow denotes $\psi^n_{f\text{pp}}$.

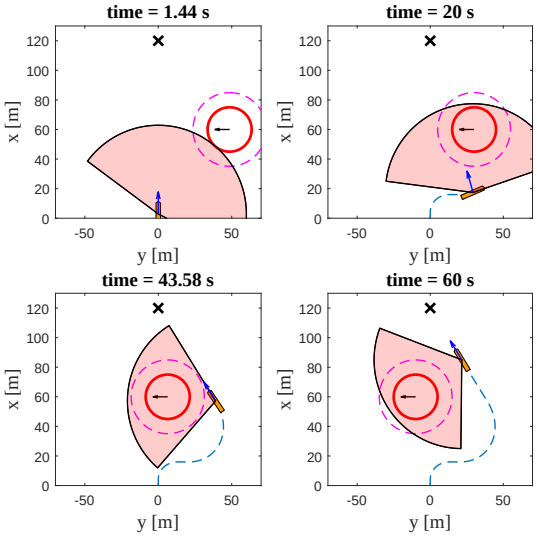

Fig. 10. The second scenario, where the obstacle crosses from starboard.

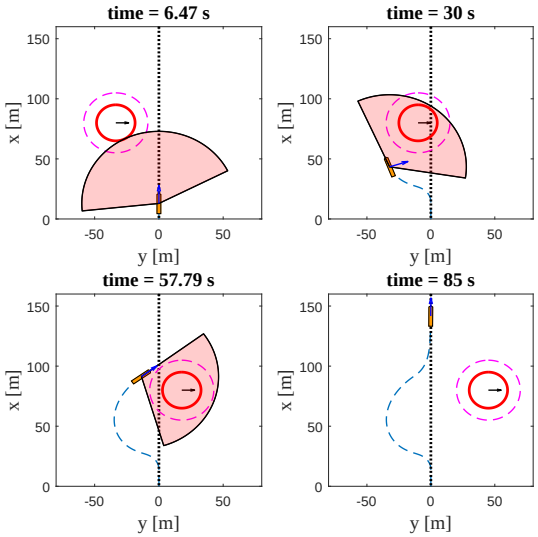

Fig. 11. The third scenario, where the obstacle crosses from port and the vehicle follows a straight line path marked by the dotted black line. The blue arrow here denotes ψ^n_{flos}.

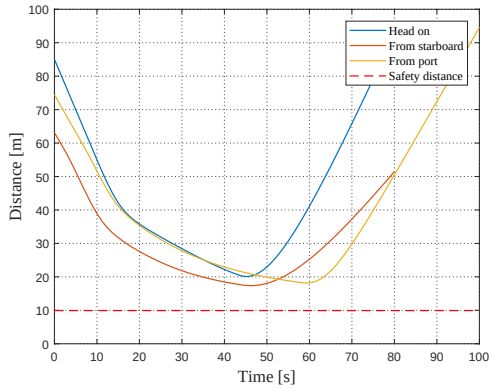

Fig. 12. The distance from the vehicle to the obstacle during the three scenarios.

ψ^n_{flos} becomes safe again. At this point, the vehicle converges to the path as stated in Theorem 2.

The obstacle distance during the three scenarios is shown in Fig. 12, where it can be seen that the distance is always above the safety distance d_{safe}. In Fig. 13, the sway velocity of the vehicle during the three scenarios are shown. The magnitude of the vehicle sway increases as the vehicle turns, but remains well below the limit of $2\,\text{m/s}$. Hence, the simulations validate the results of Theorems 1 and 2.

While the analysis in Section VIII assumes that the obstacle is circular, the CAA collision avoidance algorithm can be applied to obstacles of any shape. This is demonstrated in the fourth scenario, shown in Fig. 14, where the obstacle has the shape of a ship that is $70\,\text{m}$ long and $10\,\text{m}$ wide. The ship approaches the vehicle from the north east, and again the vehicle moves safely behind the obstacle in order to avoid it.

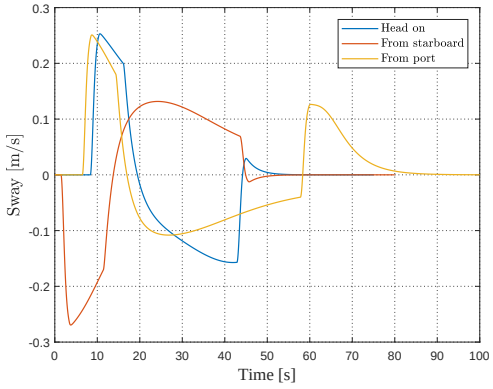

Fig. 13. The vehicle sway during the three scenarios.

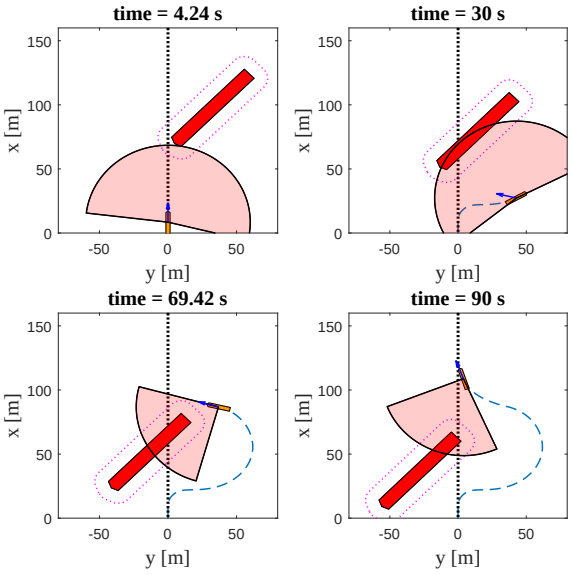

Fig. 14. The fourth scenario, where the obstacle is ship shaped.

X. Experimental Results

The CAA algorithm was implemented into the control system of the research vessel R/V Gunnerus as part of an experimental setup. The R/V Gunnerus, a research vessel owned and operated by the Norwegian University of Science and Technology (NTNU), is a $31.25\,\text{m}$ long vehicle steered by two azimuth thrusters. The control system is a Kongsberg Maritime K-Pos DP-11 system. Further details on the R/V Gunnerus can be found in [35]. The CAA collision avoidance algorithm (Section IV) and the LOS path following guidance law (Section V-B) were implemented at the guidance level of the K-Pos DP-11 system. Our algorithm thus provided heading references to an underlying heading controller, which included smoothing and control allocation. The details of the heading controller was not available to us, but the modular nature of both the CAA and LOS algorithm still made it possible to implement and tune the algorithms. We received measurements of all vehicle states, and added a simple low-pass filter to the surge and sway measurements in order to filter out the effect

of waves. The heading controller allowed us to set a maximum turning rate, which was set to $90\,^\circ/\mathrm{s}$. The speed controller was not available in this experimental mode, and the thrust level was set to a constant, providing a forward speed of about $4\,\mathrm{m/s}$.

The experiments were conducted in the Trondheim fjord. The vehicle was set to follow straight line path segments. Along the path, the vehicle encountered virtual obstacles in several different scenarios. One scenario is shown in Fig. 15, where the vehicle encountered two obstacles with a radius of $100\,\mathrm{m}$. The obstacles moved with a speed of $2\,\mathrm{m/s}$; one straight towards the vehicle slightly on its port side, and one approaching from starboard. The avoidance angle was set to $1.1\,\mathrm{rad}$, and the safety distance to $120.4\,\mathrm{m}$. At 15:07:30, the first obstacle came within a switching distance, and the vehicle turned starboard to avoid it according to the switching rule presented in Section IV-B. At 15:10:30, the second obstacle came within switching distance, and the vision cone to this obstacle was merged with the vision cone to the first. The vehicle adjusted its course to also avoid this obstacle. At 15:17:00, both obstacles had been successfully avoided and the vehicle returned to path following.

In another scenario, shown in Fig. 16, the vehicle encountered a convoy of five obstacles moving straight towards it at a speed of $2\,\mathrm{m/s}$. Again, the obstacle radius was set to $100\,\mathrm{m}$, while the avoidance angle was set to $0.9\,\mathrm{rad}$, the safety distance to $60.9\,\mathrm{m}$ and the switching distance to $800\,\mathrm{m}$. The first obstacle was encountered at 11:20:00, and the vehicle entered collision avoidance mode and turned starboard. As the vehicle moved along the convoy, it encountered the obstacles one by one and adjusted its course to avoid them. As described in Section IV-D, the turning direction was kept constant (in this case $j = 1$), thus avoiding that the vehicle tried to cross the convoy during the maneuver. The vehicle successfully avoided all five obstacles, and returned to path following.

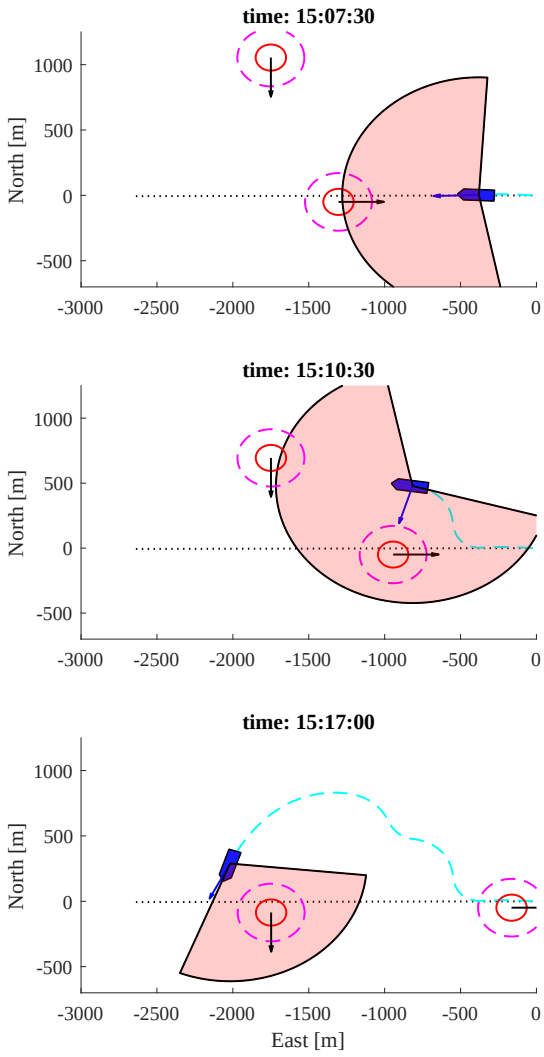

Fig. 15. Experimental run with two obstacles.

XI. Conclusions

In this paper we have proposed, and analyzed, the constant avoidance angle algorithm for collision avoidance. This algorithm is designed to make a vehicle avoid both static and moving obstacles. It creates a vision cone from the vehicle to the obstacle, extends this vision cone by a constant avoidance angle and steers the vehicle along one of the vision cone edges in order to avoid the obstacle. If the obstacle is moving, the vision cone is adjusted to exactly compensate for the obstacle velocity. The vision cone also compensates for the vehicle speed, which can thus be used as an input to the algorithm. This provides a level of flexibility which makes the algorithm suitable for vehicles with a limited speed envelope or acceleration constraints, and to vehicles operating in scenarios which put external constraints on the speed trajectory.

We have applied the algorithm to a marine vehicle with kinematics and dynamics modeled in three degrees of freedom. Specifically, we have considered the case when the vehicle has underactuated sway dynamics, which means that the sideways speed of the vehicle cannot be directly controlled, but is rather induced by turning. The CAA algorithm compensates for the underactuated sway component of the vehicle speed by steering the vehicle course. Furthermore, since we have designed the algorithm to compensate for the vehicle speed, it can readily handle the time-varying, underactuated component of the vehicle's velocity.

The CAA algorithm is modular in nature, and we demonstrated this by combining it with both the pure pursuit target reaching guidance law, and with the line-of-sight path following guidance law. We gave a mathematical analysis for both cases, and provided conditions under which it is guaranteed that the vehicle will successfully avoid an obstacle in a sparse scenario. Specifically, we provided a lower bound for the switching distance from the obstacle, at which point the vehicle should enter collision avoidance mode if it is on collision course with the obstacle. We also provided bounds on the required safety distance and course control saturation, in order to ensure that the sway movement, and hence the

Dette er en postprint-versjon/This is a postprint version. Publisert versjon/Publised version: https://doi.org/10.1109/TCST.2019.2903451

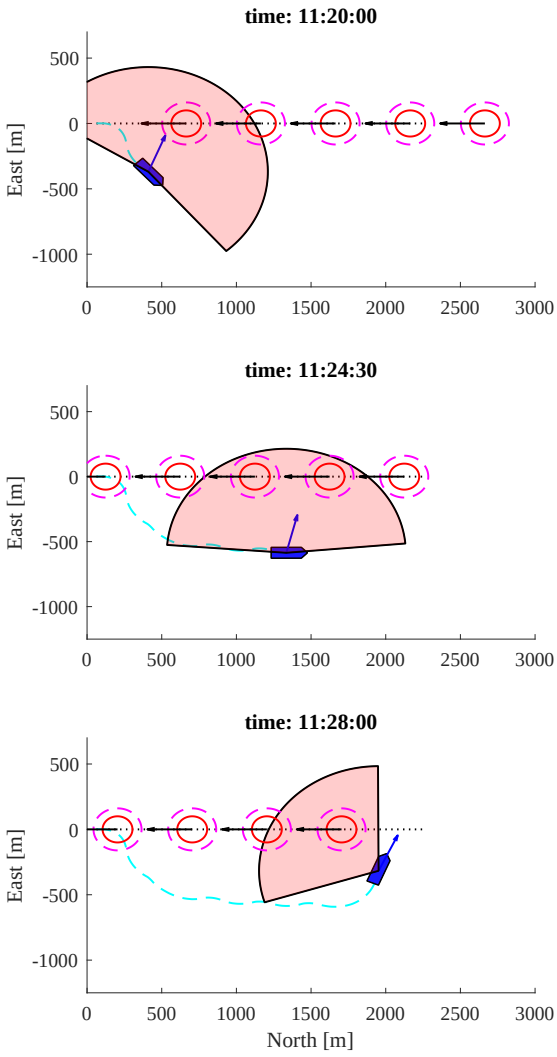

Fig. 16. Experimental run with five obstacles.

vehicle speed, remains bounded and well defined during the maneuver.

We have validated the theoretical results both by simulating an autonomous underwater vehicle operating in the plane, and in full scale experiments aboard the R/V Gunnerus. We have thus shown that the algorithm can be used on marine vessels with widely different characteristics and maneuvering capabilities. Furthermore, the experimental results indicate that the algorithm is robust to noise such as wave disturbances, as well as to operating on a vessel where the details of the low-level controllers and vehicle model are not available. Both the simulations and the experiments show that the vehicle keeps well away from the obstacle, which suggest that the conditions derived in Theorems 1 and 2 are conservative.

Finally, while the analysis in this paper assumed a sparse scenario with circular obstacles that can be avoided one at a time, we have shown in the simulations and the experiments both that the algorithm can be applied to obstacles of different shapes, and how to extend the algorithm to a multi-obstacle scenario. However, a thorough analysis of such scenarios, which would include extending the algorithm to several, cooperative agents, remains a topic of future work.

Appendix A
Functional Expressions

$$F_{u_b}(u_b, v_b, r_b) \triangleq \frac{1}{m_{11}}(m_{22}v_b + m_{23}r_b)r_b - \frac{d_{11}}{m_{11}}u_b \quad (91)$$

$$X(u_b) \triangleq \frac{m_{23}^2 - m_{11}m_{33}}{m_{22}m_{33} - m_{23}^2}u_b + \frac{d_{33}m_{23} - d_{23}m_{33}}{m_{22}m_{33} - m_{23}^2} \quad (92)$$

$$Y(u_b) \triangleq \frac{(m_{22} - m_{11})m_{23}}{m_{22}m_{33} - m_{23}^2}u_b - \frac{d_{22}m_{33} - d_{32}m_{23}}{m_{22}m_{33} - m_{23}^2} \quad (93)$$

$$F_{r_b}(u_b, v_b, r_b) \triangleq \frac{m_{23}d_{22} + m_{22}(d_{32} + (m_{22} - m_{11})u_b)}{m_{22}m_{33} - m_{23}^2}v_b + \frac{m_{23}(d_{23} - m_{11}u_b) - m_{22}(d_{33} + m_{23}u_b)}{m_{22}m_{33} - m_{23}^2}r_b$$

Acknowledgments

The authors would like to thank Dr. Signe Moe for implementing the LOS path following algorithm aboard the R/V Gunnerus, and for her help and assistance during the trials. We would also like to thank Øystein Lurås, Inge Spangelo and Bjørn Ole Vinje at Kongsberg Maritime for prividing access to their control system API, and for their invaluable support before and during the experiments. Finally, we would like to thank the crew aboard the R/V Gunnerus for accommodating us, and for bravely letting us take control of their vessel.

References

[1] V. Bertram, "Unmanned Surface Vehicles A Survey," *Skibsteknisk Selskab, Copenhagen, Denmark*, 2008.
[2] Z. Liu, Y. Zhang, X. Yu, and C. Yuan, "Unmanned surface vehicles: An overview of developments and challenges," *Annual Reviews in Control*, vol. 41, pp. 71–93, 2016.
[3] T. I. Fossen, *Handbook of marine craft hydrodynamics and motion control*. John Wiley & Sons, 2011.
[4] T. Statheros, G. Howells, and K. M. Maier, "Autonomous Ship Collision Avoidance Navigation Concepts, Technologies and Techniques," *Journal of Navigation*, vol. 61, no. 01, pp. 129–142, 2008.
[5] C. Tam, R. Bucknall, and A. Greig, "Review of Collision Avoidance and Path Planning Methods for Ships in Close Range Encounters," *The Journal of Navigation*, vol. 62, no. 2009, pp. 455–476, 2009.
[6] M. Hoy, A. S. Matveev, and A. V. Savkin, "Algorithms for collision-free navigation of mobile robots in complex cluttered environments: a survey," *Robotica*, vol. 33, no. 03, pp. 463–497, 2014.
[7] I. B. Hagen, D. K. M. Kufoalor, E. F. Brekke, and T. A. Johansen, "MPC-based collision avoidance Strategy for existing marine vessel guidance systems," in *Proc. IEEE International Conference on Robotics & Automation (ICRA)*, (Brisbane, Australia), 2018.
[8] T. A. Johansen, T. Perez, and A. Cristofaro, "Ship collision avoidance and COLREGS compliance using simulation-based control behavior selection with predictive hazard assessment," *IEEE Transactions on Intelligent Transportation Systems*, vol. 17, no. 12, pp. 3407–3422, 2016.
[9] Y. Chen, H. Peng, and J. Grizzle, "Obstacle avoidance for low-speed autonomous vehicles with barrier function," *IEEE Transactions on Control Systems Technology*, vol. 26, no. 1, pp. 194–206, 2018.
[10] D. Fox, W. Burgard, and S. Thrun, "The dynamic window approach to collision avoidance," *IEEE Robotics and Automation Magazine*, vol. 4, no. 1, pp. 23–33, 1997.

[11] B. O. H. Eriksen, M. Breivik, K. Y. Pettersen, and M. S. Wiig, "A modified dynamic window algorithm for horizontal collision avoidance for AUVs," in *Proc. 2016 IEEE Conference on Control Applications (CCA)*, (Buenos Aires, Brazil), pp. 499–506, 2016.

[12] B. O. H. Eriksen, E. F. Wilthil, A. L. Flåten, E. F. Brekke, and M. Breivik, "Radar-based maritime collision avoidance using dynamic window," in *IEEE Aerospace Conference Proceedings*, (Big Sky, MT, USA), 2018.

[13] J. Canny and J. Reif, "New lower bound techniques for robot motion planning problems," in *Proc. 28th Annual Symposium on Foundations of Computer Science*, (Los Angeles, CA, USA), pp. 49–60, 1987.

[14] O. Khatib, "Real-time obstacle avoidance for manipulators and mobile robots," *The International Journal of Robotics Research*, vol. 5, no. 1, pp. 90–98, 1986.

[15] T. Paul, T. R. Krogstad, and J. Tommy, "Modelling of UAV formation flight using 3D potential field," *Simulation Modelling Practice and Theory*, vol. 16, no. 9, pp. 1453–1462, 2008.

[16] Y. Koren and J. Borenstein, "Potential field methods and their inherent limitations for mobile robot navigation," in *Proc. IEEE International Conference on Robotics and Automation (ICRA)*, (Sacramento, CA, USA), pp. 1398–1404, 1991.

[17] J. Borenstein and Y. Koren, "The vector field histogram–Fast obstacle avoidance for mobile robots," *IEEE Transactions on Robotics and Automation*, vol. 7, no. 3, pp. 278–288, 1991.

[18] P. Fiorini and Z. Shiller, "Motion planning in dynamic environments using velocity obstacles," *The International Journal of Robotics Research*, vol. 17, no. 7, pp. 760–772, 1998.

[19] Y. Kuwata, M. T. Wolf, D. Zarzhitsky, and T. L. Huntsberger, "Safe maritime autonomous navigation with COLREGS, using velocity obstacles," *IEEE Journal of Oceanic Engineering*, vol. 39, no. 1, pp. 110–119, 2014.

[20] J. van den Berg, J. Snape, S. J. Guy, and D. Manocha, "Reciprocal collision avoidance with acceleration-velocity obstacles," in *Proc. IEEE International Conference on Robotics and Automation (ICRA 2011)*, (Shanghai, China), pp. 3475–3482, 2011.

[21] D. Wilkie, J. Van Den Berg, and D. Manocha, "Generalized velocity obstacles," in *Proc. IEEE/RSJ International Conference on Intelligent Robots and Systems,*, (St. Louis, MA, USA), pp. 5573–5578, 2009.

[22] E. Lalish and K. A. Morgansen, "Decentralized Reactive Collision Avoidance for Multivehicle Systems," in *Proc. 47th IEEE Conference on Decision and Control Decision Control*, (Cancun, Mexico), 2008.

[23] A. Chakravarthy and D. Ghose, "Obstacle avoidance in a dynamic environment: A collision cone approach," *IEEE Transactions on Systems, Man, and Cybernetics Part A:Systems and Humans.*, vol. 28, no. 5, pp. 562–574, 1998.

[24] S. Moe and K. Y. Pettersen, "Set-Based Line-of-Sight (LOS) Path Following with Collision Avoidance for Underactuated Unmanned Surface Vessels under the Influence of Ocean Currents," in *Proc. 1st IEEE Conference on Control Technology and Applications*, (Kohala Coast, HI, USA), 2017.

[25] K. Pettersen and E. Lefeber, "Way-point tracking control of ships," in *Proc. 40th IEEE Conference on Decision and Control*, (Orlando, FL), pp. 940–945, 2001.

[26] A. V. Savkin and C. Wang, "A simple biologically inspired algorithm for collision-free navigation of a unicycle-like robot in dynamic environments with moving obstacles," *Robotica*, vol. 31, no. 6, pp. 993–1001, 2013.

[27] M. S. Wiig, K. Y. Pettersen, and A. V. Savkin, "A reactive collision avoidance algorithm for nonholonomic vehicles," in *Proc. 1st IEEE Conference on Control Technology and Applications*, (Kona, HI, USA), 2017.

[28] M. S. Wiig, K. Y. Pettersen, and T. R. Krogstad, "A reactive collision avoidance algorithm for vehicles with underactuated dynamics," in *Proc. 56th IEEE Conference on Control Technology and Applications*, (Melbourne, Australia), 2017.

[29] A. Healey and D. Lienard, "Multivariable sliding mode control for autonomous diving and steering of unmanned underwater vehicles," *IEEE Journal of Oceanic Engineering*, vol. 18, no. 3, pp. 327–339, 1993.

[30] M. Breivik and T. I. Fossen, "Guidance laws for planar motion control," in *Proc. IEEE Conference on Decision and Control*, (Cancun, Mexico), pp. 570–577, 2008.

[31] T. I. Fossen and K. Y. Pettersen, "On uniform semiglobal exponential stability (USGES) of proportional line-of-sight guidance laws," *Automatica*, vol. 50, no. 11, pp. 2912–2917, 2014.

[32] E. Borhaug and K. Y. Pettersen, "LOS path following for underactuated underwater vehicle," in *Proc. 7th IFAC Conference on Manoeuvring and Control of Marine Craft*, (Lisbon, Portugal), 2006.

[33] E. Børhaug, A. Pavlov, E. Panteley, and K. Y. Pettersen, "Straight line path following for formations of underactuated surface vessels," *IEEE Transactions on Control Systems Technology*, vol. 19, no. 3, pp. 493–506, 2011.

[34] P. E. Hagen, N. Storkersen, K. Vestgard, and P. Kartvedt, "The HUGIN 1000 autonomous underwater vehicle for military applications," in *Proc. Oceans 2003*, (San Diego, CA, USA), pp. 1141–1145, 2003.

[35] R. Skjetne, M. E. N. Sørensen, M. Breivik, S. A. T. Værnø, A. H. Brodtkorb, A. J. Sørensen, Ø. K. Kjerstad, V. Calabrò, and B. O. Vinje, "AMOS DP research cruise 2016: academic full-scale testing of experimental dynamic positioning control algorithms onboard R/V Gunnerus," in *Proc. ASME 36th Int. Conf. Ocean, Offshore Arctic Eng*, (Trondheim, Norway), 2017.

Martin Syre Wiig received the M.Sc. in engineering cybernetics from the Norwegian University of Science and Technology (NTNU), Trondheim, Norway, in 2007. Since 2007, he has been with the Norwegian Defense Research Establishment (FFI), where he is currently a Senior Scientist. At FFI, he works on decisional autonomy for unmanned vehicles and modelling and control of marine vehicles. In 2014 he started as a PhD student at NTNU, where he is currently working on path following and collision avoidance of underactuated marine vehicles.

Kristin Ytterstad Pettersen (F17) received the M.Sc. and Ph.D. degrees in engineering cybernetics from the Norwegian University of Science and Technology (NTNU), Trondheim, Norway, in 1992 and 1996, respectively. Since 1996, she has been a Faculty Member with the Department of Engineering Cybernetics, NTNU, where she is currently a Professor. She was the Director of the NTNU ICT Programme of Robotics from 2010 to 2013, the Vice-Head of the Department from 2009 to 2011, and the Head of Department from 2011 to 2013. She is an Adjunct Professor with the Norwegian Defence Research Establishment (FFI). She is also a Key Scientist with the CoE Centre for Autonomous Marine Operations and Systems, NTNU, for 20132022. She is a Co-Founder of the NTNU spin-off company Eelume AS, where she was the CEO from 2015 to 2016. She has published four books and over 250 papers in scientific conferences and journals. Her current research interests include nonlinear control of mechanical systems with applications to robotics, with a special emphasis on marine robotics and snake robotics.

Dr. Pettersen was a member of the Board of Governors of IEEE Control Systems Society from 2012 to 2014. She is a member of the IFAC Council, the Norwegian Academy of Technological Sciences, and the Academy of the Royal Norwegian Society of Sciences and Letters. She has also held and holds several board positions in industrial and research companies. She was a recipient of the IEEE TRANSACTIONS ON CONTROL SYSTEMS TECHNOLOGY Outstanding Paper Award in 2006 and 2017, respectively.

Thomas Røbekk Krogstad received the M.Sc. and Ph.D. degree in engineering cybernetics from the Norwegian University of Science and Technology (NTNU), Trondheim, Norway, in 2005 and 2010, respectively. Since 2009, he has been with the Norwegian Defense Research Establishment (FFI) where he is currently a Senior Scientist. His current research interests include decisional autonomy and guidance and control of unmanned marine vehicles.